Journal of Peptide Science
J. Peptide Sci. **11**: 29–36 (2005)
Published online 23 August 2004 in Wiley InterScience (www.interscience.wiley.com). DOI: 10.1002/psc.589

JOURNAL OF PEPTIDE SCIENCE

Design, NMR characterization and activity of a 21-residue peptide fragment of bacteriocin AS-48 containing its putative membrane interacting region

M. ANGELES JIMÉNEZ,[a]* ANA C. BARRACHI-SACCILOTTO,[a] EVA VALDIVIA,[b] MERCEDES MAQUEDA[b] and MANUEL RICO[a]

[a] Instituto de Química-Física Rocasolano, Consejo Superior de Investigaciones Científicas, Serrano 119, 28006-Madrid, Spain
[b] Departamento de Microbiología, Facultad de Ciencias, Universidad de Granada, C/Fuentenueva s/n, 18071-Granada, Spain

Received 22 January 2004; *Revised 26 February 2004*; *Accepted 28 April 2004*

Abstract: Bacteriocin AS-48 is a 70-residue cyclic polypeptide from *Enterococcus faecalis* that shows a broad antimicrobial spectrum against both Gram-positive and Gram-negative bacteria. The structure of bacteriocin AS-48 consists of a globular arrangement of five helices with a high positive electrostatic potential in the region comprising helix 4, the turn linking helix 4 and 5, and the *N*-terminus of helix 5. This region has been considered to participate in its biological activity and in particular in membrane permeation. To understand the mechanism of the antibacterial activity of AS-48 and to discriminate the several mechanisms proposed, a simplified bacteriocin was designed consisting of 21 residues and containing the high positively charged region. A disulfide bridge was introduced at an appropriate position to stabilize the peptide and to conserve the helix-turn-helix arrangement in the parent molecule. According to ^{1}H and ^{13}C NMR data, the designed simplified bacteriocin fragment adopts a significant population of a native-like helical hairpin conformation in aqueous solution, which is further stabilized in 30% TFE. The designed peptide does not show any antibacterial activity, though it is shown to compete with the intact native bacteriocin AS-48. These results suggest that the mechanism of membrane disruption by bacteriocin is not as simple as being driven by a deposition of positively charged molecules on the plane of the bacterial membrane. Some other regions of the protein must be present such as, for instance, hydrophobic regions so as to enhance the accumulation of the peptide and favour membrane permeation.

Keywords: antimicrobial activity; ^{1}H NMR; ^{13}C NMR; peptide structure

INTRODUCTION

The need to find and develop novel antibiotic agents is becoming more urgent as a consequence of the increase in the levels of bacterial resistance to current antibiotics experienced over the past decade. In this sense, naturally occurring cationic antimicrobial peptides constitute an alternative source of bactericidal agents by themselves and as the basis for new designs [1,2]. Bacteriocin AS-48 is a 70-residue cyclic polypeptide isolated from *Enterococcus faecalis* [3,4] that shows a broad antimicrobial spectrum against both Gram-positive and Gram-negative bacteria [5]. Permeation of the cell membrane leading to cell death is the accepted mechanism for the action of a large number of membrane-lytic polypeptides such as AS-48. Molecular electroporation refers to pore formation into membranes caused by a sufficiently high external magnetic field produced by the binding of a charged molecule to the surface of the membrane. The structure of bacteriocin AS-48 has been determined by NMR, and consists of a globular arrangement of five helices [6], in which the region comprising helix α_4, the turn linking helix α_4 and α_5, and the *N*-terminus of helix α_5 displays a high positive electrostatic potential, to which has been ascribed its ability to interact with the negatively charged bacterial membrane, leading ultimately to electroporation. A similar five-helix structural motif has been found in the antimicrobial NK-lysin [7], an antibacterial and tumourolytic 78-residue polypeptide of T and natural killer (NK) cells, isolated from porcine small intestine. As for bacteriocin AS-48, NK-lysin shows a high electropositive potential, though the orientation of the direction of maximum potential with respect to the five-helix bundle is quite different. Thus, some analogies and some differences are expected in relation to their biological activity. More recently, the crystal structure of bacteriocin at a higher pH has been determined [8]. Whereas the single molecules appear as five-helix bundles as observed by NMR, they are arranged in chains of pairs of molecules linked either by hydrophobic interactions (dimer DF-1) or by hydrophilic interactions (dimer DF-2). On the basis of the existence of these two different dimers, a mechanism of action has been proposed by which the soluble dimer (DF-1) approaches the

*Correspondence to: Dr M. Angeles Jiménez, Instituto de Química-Física Rocasolano, Consejo Superior de Investigaciones Científicas, Serrano 119, 28006-Madrid, Spain; e-mail: majimenez@iqfr.csic.es
Contract/grant sponsor: Spanish DGICYT; Contract/grant number: PB98-0677.
Contract/grant sponsor: European Union; Contract/grant number: CEE B104-97-2086.

membrane surface driven by electrostatic forces, then it rearranges to the alternative dimer (DF-2), which finally penetrates partially into the membrane. In order better to understand the mechanism of the antibacterial activity of AS-48 and to discriminate the several mechanisms proposed, it was decided to design a simplified bacteriocin consisting of just 21 residues containing the high positively charged region, which putatively interacts with bacterial membranes. This decision was encouraged by the positive results obtained by Andreu *et al.* [9] in the identification of an anti-mycobacterial domain in NK-lysin and granulysin, consisting of a 22-residue fragment peptide. Here, the NMR structure adopted by the 21-residue simplified bacteriocin AS-48 fragment peptide and its biological activity is reported.

MATERIALS AND METHODS

Peptide Synthesis and Purification

B-49-69 was chemically synthesized by DiverDrugs (Barcelona, Spain). Deuterated TFE was purchased from Cambridge Isotope Laboratory.

Sedimentation Equilibrium

Sedimentation equilibrium experiments were performed on a sample of approximately 0.2 mM concentration in aqueous solution at pH 5.5 and containing 150 mM NaCl to screen non-ideal effects involving charged residues at high peptide concentrations. The peptide sample (100 µl) was centrifuged at 60 000 rpm at 278K in 12 mm triple-sector Epon charcoal centrepieces, using a Beckman Optima XL-A ultracentrifuge with a Ti60 rotor. Radial scans were taken at different wavelengths every 2 h until equilibrium conditions were reached. The data were analysed using the XLAEQ program from Beckman. The partial specific volumes of the peptides were calculated on the basis of their amino acid composition and corrected for temperature [10].

NMR Spectra

Peptide samples for NMR experiments were prepared in 0.5 ml of H_2O/D_2O (9 : 1 ratio by volume) or in pure D_2O. Peptide concentrations were about 1–2 mM. pH was measured with a glass microelectrode and was not corrected for isotope effects. The temperature of the NMR probe was calibrated using a methanol sample. Sodium [3-trimethylsilyl 2,2,3,3-$^2H_4$] propionate (TSP) was used as an internal reference. The ^{1}H-NMR spectra were acquired on a Bruker AMX-600 pulse spectrometer operating at a proton frequency of 600.13 MHz. 1D spectra were acquired using 32K data points, which were zero-filled to 64K data points before performing the Fourier transformation. Phase-sensitive two-dimensional correlated spectroscopy (COSY; [11]) total correlated spectroscopy (TOCSY; [12]) and nuclear Overhauser enhancement spectroscopy (NOESY; [13,14]) spectra were recorded by standard techniques using presaturation of the water signal and the time-proportional phase incrementation mode [15]. The NOESY and ROESY mixing times were 200 ms and 120 ms, respectively. TOCSY spectra were recorded using 80 ms MLEV17 with z filter spin-lock sequence [12]. The ^{1}H-^{13}C heteronuclear single quantum coherence spectra (HSQC; [16]) at natural ^{13}C abundance were recorded in 2 mM peptide samples in D_2O or in 30 : 70 TFE/D_2O (v/v). Acquisition data matrices were defined by 2018 × 512 points in t_2 and t_1, respectively. Data were processed using the standard XWIN-NMR Bruker program on a Silicon Graphics computer. The 2D data matrix was multiplied by a square-sine-bell window function with the corresponding shift optimized for every spectrum and zero-filled to a 2 K × 1 K complex matrix prior to Fourier transformation. Baseline correction was applied in both dimensions. The 0 ppm ^{13}C δ was obtained indirectly by multiplying the spectrometer frequency that corresponds to 0 ppm in the ^{1}H spectrum, assigned to internal TSP reference, by 0.25144954 [17,18].

NMR Assignment

The ^{1}H NMR signals of B-49-69 in aqueous solution and in the mixed solvent 30 : 70 TFE/H_2O were readily assigned by standard sequential assignment methods [19,20]. Then, the ^{13}C resonances were straightforwardly assigned on the basis of the cross-correlations observed in the HSQC spectra between the proton and the carbon to which it is bonded. The ^{1}H and ^{13}C δ-values of B-49-69 in aqueous solution and in 30 : 70 TFE/H_2O are available as Supplementary Material (Tables SM1 and SM2).

Estimation of Helix Populations

Helix populations were quantified from C_αH proton and $^{13}C_\alpha$ carbon δ-values. The method based on C_αH proton δ-values was previously described [21,22] and an analogous procedure, equivalent to that described for evaluating β-sheet populations [23], was followed by using $^{13}C_\alpha$ carbon δ-values. To obtain the helix percentage, the $\Delta\delta_{C\alpha H}$ ($\Delta\delta_{C\alpha H} = \delta_{C\alpha H}{}^{\text{observed}} - \delta_{C\alpha H}{}^{\text{random coil}}$, ppm) and $\Delta\delta_{C\alpha}$ ($\Delta\delta_{C\alpha} = \delta_{C\alpha}{}^{\text{observed}} - \delta_{C\alpha}{}^{\text{random coil}}$, ppm) values averaged for all the helical residues were divided by the $\Delta\delta_{C\alpha H}$ and $\Delta\delta_{C\alpha}$ values corresponding to 100% helix, −0.39 ppm [24] and +3.09 ppm [18], respectively, and then multiplied by 100. The random coil C_αH δ-values ($\delta_{C\alpha H}{}^{\text{random coil}}$) were taken from Wüthrich [20] and the random coil $^{13}C_\alpha$ δ-values ($\delta_{C\alpha}{}^{\text{random coil}}$) from Merutka *et al.* [25].

Structure Calculation

Distance constraints for structure calculations were derived from the 2D 150 ms mixing time NOESY spectra recorded either in H_2O and in D_2O or in 30 : 70 TFE/H_2O and in 30 : 70 TFE/D_2O. The NOE cross-peaks were integrated by using the automatic integration subroutine of the X-EASY program [26] and then calibrated and converted to upper limit distance constraints within the DYANA program [27]. ϕ and ψ angle restraints were derived from $^1H_\alpha$, $^{13}C_\alpha$ and $^{13}C_\beta$ chemical shifts by using the TALOS program [28]. ϕ angles for those residues for which the derived angle restraints were ambiguous were constrained to the range −180° to 0°, except for Asn and Gly residues. Structures were calculated using the DYANA program [27] and an annealing strategy.

Structure Analysis

Model structures calculated for B-49-69 as well as those previously reported for bacteriocin AS-48 in solution (pdb code: 1e68; [6]) and in the crystalline state (pdb codes: 1o82, 1o83, 1o84; [8]) were examined by using the program MOLMOL [29].

Biological Activity and Neutralization Assays

Assays were performed in both solid and liquid media. Activity tests in a solid medium were done by the drop technique as follows: samples (2.5 or 5 µl) of semipurified bacteriocin AS-48 with a known protein concentration (12.5 µg/ml in distilled water) and samples (5 µl or 10 µl) of B-49-69 (44 mg/ml) dissolved in distilled water (pH 6.5) or *ortho*-phosphoric acid buffer (pH 5), were spotted onto plates of brain hearth infusion agar (BHA, Scharlab, Barcelona, Spain) previously overlaid with 5 ml of BHA soft-agar inoculated with the indicator strain *Listeria monocytogenes* CECT 4032 (approx. 10^8 colony forming units, CFU). After incubation for 18 h at 37 °C, the inhibition halos on the seeded lawn were visualized. An antilisterial activity test in liquid medium was carried out as follows: AS-48 (0.05 µg/ml) was added to cultures growing in BHI broth at 37 °C, with an optical density at 620 nm ca. 0.1 (approx. 5×10^7 CFU/ml). At desired intervals, growth and lysis were monitored turbidimetrically in a LKB Ultrospec III spectrophotometer (Pharmacia-Biotech).

B-49-69/AS-48 neutralization experiments in solid media were carried out as described above for the AS-48 biological activity test, but before the addition of AS-48, drops containing 110 µg of B-49-69 at pH 5 or 6.5 were spotted on the plates seeded with the indicator strain and incubated for 2 h at 37 °C, in order to allow peptide adsorption to *Listeria* cells. For neutralization experiments in liquid media, exponential cultures of indicator strain were treated with B-49-69 (220 µg/ml) and maintained at 37 °C for 30 min, before AS-48 treatment and then processed as above.

Dotblotting Immunological Detection

1 µl of a sample containing 44 µg of B-49-69 was adsorbed onto a nitrocellulose (NC) sheet (Schleicher and Schuell; 0.45 µm pore size BA85) and then processed by dot immunoassay [30]. Proteins bound to NC were visualized after having first been reacted with the primary AS-48 specific antibodies (1/100) dilution [31] and then with horseradish peroxidase-labelled secondary antibodies (1/1000 dilution; Institut Pasteur, Paris, France). A parallel positive control with bacteriocin AS-48 (1 µg) was performed.

RESULTS

Peptide Design

To design a simplified bacteriocin AS-48 with putative bactericidal activity the segment 49–69 was selected comprising helix 4 and the *N*-terminal region of helix 5, where the large patch of positive charges is located, and where the antibiotic activity of bacteriocin AS-48 was proposed to reside (Figure 1; [6]). To avoid charge effects, the *N*-terminal amino group was acetylated and the *C*-terminal carboxylate group amidated. In trying to maintain the relative orientation of the helices in the isolated fragment, residues I59 and V67, whose side chains interact in the intact bacteriocin AS-48 (Figure 1) were substituted for Cys and linked by a disulfide bond. The C59–C67 disulfide bond was expected to contribute to fix the arrangement between the two helices. The final designed minimal bacteriocin AS-48, (I59C, V67C)-bacteriocin-49-69, is named B-49-69 hereafter.

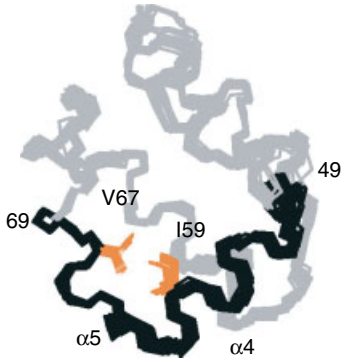

Figure 1 Superposition of the backbone atoms for the 20 best NMR structures of bacteriocin AS-48 (pdb code: 1e68; [6]). Backbone atoms of segment 49–69 are shown in black. I59 and V67 side chains are displayed in orange.

State of Association

Line widths and signal chemical shifts measured in the 1D ^{1}H NMR spectra of B-49-69 in aqueous solution at two different concentrations, 2 mM and 0.2 mM, were identical, indicating that the peptide does not aggregate. Its monomeric state was further confirmed by the similarity between the average molecular weight (M_{av}) obtained from sedimentation equilibrium experiments performed with the dilute sample and the molecular weight (M_{th}) calculated on the basis of the amino acid composition ($M_{th}/M_{av} = 0.84$).

NMR Structural Study

The structure adopted by B-49-69 in aqueous solution and in the mixed solvent 30 : 70 TFE/H_2O (v/v) was investigated by analysis of several NMR parameters, NOE connectivities, and ^{1}H and ^{13}C chemical shifts (δ). Two helices, a long one extending from residue 49 to 61 and a short one spanning residues 64–68, are clearly delineated on the basis of the stretches of non-sequential $d_{\alpha N(i,i+2)}$, $d_{\alpha N(i,i+3)}$, $d_{\alpha N(i,i+4)}$, $d_{\alpha\beta(i,i+3)}$ and $d_{NN(i,i+2)}$ NOE connectivities, negative $\Delta\delta_{C\alpha H}$ values ($\Delta\delta_{C\alpha H} = \delta_{C\alpha H}^{\text{observed}} - \delta_{C\alpha H}^{\text{random coil}}$, ppm), positive $\Delta\delta_{C\alpha}$ values ($\Delta\delta_{C\alpha} = \delta_{C\alpha}^{\text{observed}} - \delta_{C\alpha}^{\text{random coil}}$, ppm) and negative $\Delta\delta_{C\beta}$ values ($\Delta\delta_{C\beta} = \delta_{C\beta}^{\text{observed}} - \delta_{C\beta}^{\text{random coil}}$, ppm) observed for B-49-69 (Figures 2, 3). NOE correlations i, i + 3 and i, i + 4 involving side chain protons are also compatible with the presence of the two helices. Based

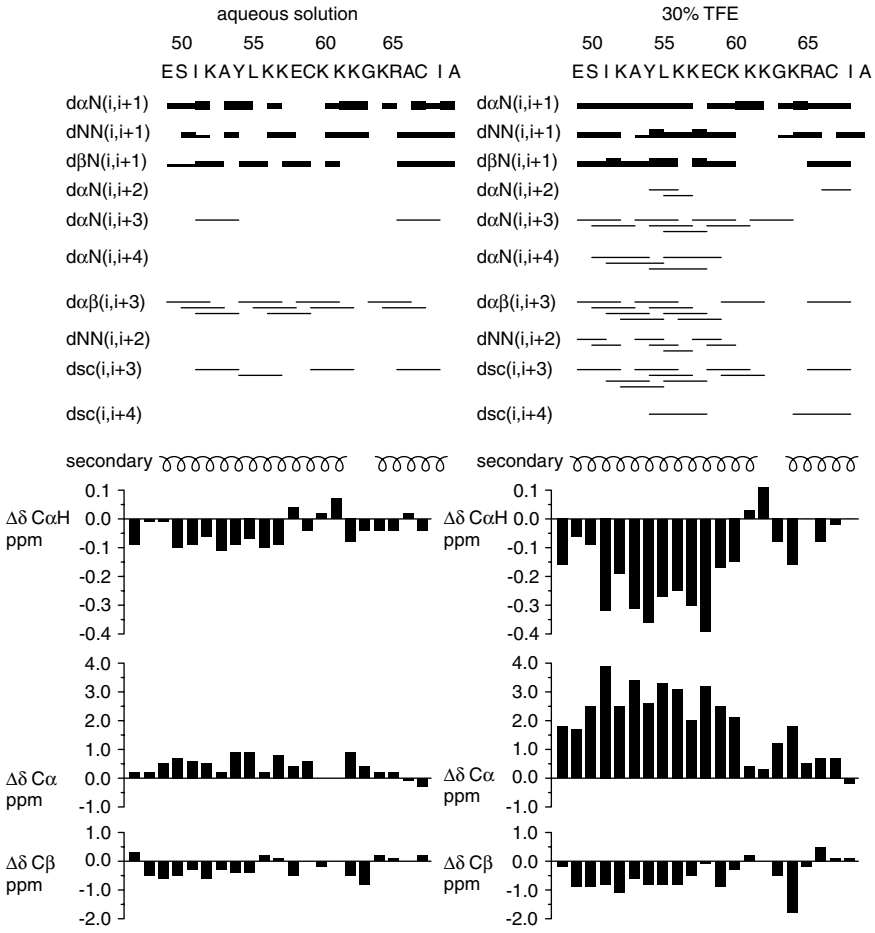

Figure 2 Summary of NOE connectivities and histograms of $\Delta\delta_{C\alpha H}$ values ($\Delta\delta_{C\alpha H} = \delta_{C\alpha H}{}^{observed} - \delta_{C\alpha H}{}^{random\ coil}$, ppm), $\Delta\delta_{C\alpha}$ values ($\delta_{C\alpha}{}^{observed} - \delta_{C\alpha}{}^{random\ coil}$, ppm) and $\Delta\delta_{C\beta}$ values ($\delta_{C\beta}{}^{observed} - \delta_{C\beta}{}^{random\ coil}$, ppm) as a function of sequence for B-49-69 in D_2O (left) and in 30 : 70 TFE/D_2O (right) at pH 5.5 and 25 °C. The thickness of the lines reflects the intensity of the sequential NOE connectivities, classified as weak, medium and strong. NOE connectivities involving sidechain protons are indicated as d_{sc}. The averaged $\Delta\delta_{C\alpha H}$ value is shown for Gly residues. $\delta_{C\alpha H}{}^{random\ coil}$ values were taken from Wüthrich [37] and $\delta_{C\alpha}{}^{random\ coil}$ and $\delta_{C\beta}{}^{random\ coil}$ values from Merutka *et al.* [38]. Extension of the α-helices is indicated in the middle.

on the $\Delta\delta_{C\alpha H}$ and $\Delta\delta_{C\alpha}$ values averaged for the residues corresponding to each helix ([21,22]; see Materials and Methods), the populations of the *N*-terminal and *C*-terminal helices are 16% and 13%, respectively, in aqueous solution at pH 5.5 and 5 °C. In the presence of TFE, the larger number of non-sequential NOEs characteristic of helices and the larger $\Delta\delta_{C\alpha H}$, $\Delta\delta_{C\alpha}$ and $\Delta\delta_{C\beta}$ values in absolute value observed relative to aqueous solution are clear evidence that the two helices, in particular the longest *N*-terminal one, have increased their populations. The corresponding populations for the *N*-terminal and *C*-terminal helices in the presence of 30% TFE are 75% and 27%, respectively, at pH 5.5 and 25 °C (Table 1). In both solvent conditions, B-49-69 exists in a conformational equilibrium consisting of (i) helical hairpins, peptide molecules with the two helices formed, (ii) peptide molecules where the *N*-terminal helix, but not the *C*-terminal one, is formed, (iii) peptide molecules with the *N*-terminal helix disordered but with the *C*-terminal helix formed, and (iv) the random coil state.

Structure Calculation

Because of the conformational equilibrium present in B-49-69, as commonly occurs in peptides, NOE data cannot be interpreted in terms of a single structure. Nevertheless, the calculation of a limited number of structures compatible with the observed NOEs is a common and useful way to visualize the features of the favoured family of structures present in the conformational ensemble of a peptide. Therefore, to gain some insights into the native-likeness of the B-49-69 helical hairpins, two B-49-69 model structures were calculated, one in aqueous solution and the other in 30% TFE, by using distance restraints derived from the intensities of the sequential NH_i-NH_{i+1} and non-sequential NOEs (a total of 53 in water and 110 in 30% TFE). Intraresidual and sequential NOEs, apart

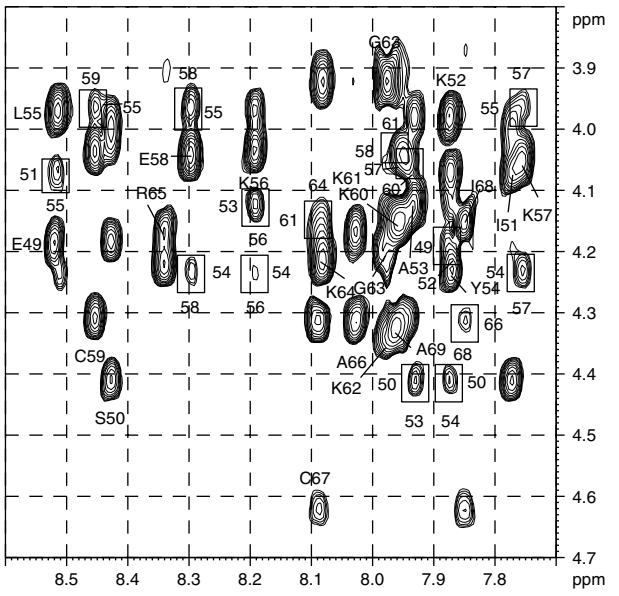

Figure 3 Selected region of NOESY spectra of B-49-69 in 30% TFE at pH 5.5 and 25 °C. Intra-residual $d_{\alpha N(i,i)}$ NOE cross-peaks are labelled and non-sequential $d_{\alpha N(i,i+2)}$, $d_{\alpha N(i,i+3)}$ and $d_{\alpha N(i,i+4)}$ NOE cross-peaks are boxed and labelled.

Table 1 Helix Populations Estimated for B-49-69 in Aqueous Solution at pH 5.5 and 5 °C and in 30% TFE at pH 5.5 and 25 °C as described at Methods

	Aqueous solution		30% TFE	
Helix residues	50–61	64–68	50–61	54–68
Averaged helix population, %	**16 ± 1**	**13 ± 1**	**75 ± 19**	**27 ± 7**
$\Delta\delta_{C\alpha H}$, ppm[a]	−0.06	−0.05	−0.238	−0.085
Helix population[b], %	15.4	12.8	61.0	21.8
$\Delta\delta_{C\alpha}$, ppm[c]	+0.54	+0.425	+2.73	+0.98
Helix population[d], %	17.5	13.8	88.3	31.7

[a] $\Delta\delta_{C\alpha H}$ value averaged for the helical residues.
[b] Estimated from $\Delta\delta_{C\alpha H}$ values.
[c] $\Delta\delta_{C\alpha}$ value averaged for the helical residues.
[d] Estimated from $\Delta\delta_{C\alpha}$ values.

from the NH_i-NH_{i+1} NOEs, were excluded due to the contribution of random coil conformations to their intensities. This contribution is negligible in the case of the sequential NH_i-NH_{i+1} NOEs, which were included in the calculation, because they are very far apart in any conformation except for helices and turns. The NOEs contributing to defining the inter helical angle are those involving a proton of a residue in helix 50–61 and a proton of a residue in helix 64–68, i.e. those between the two disulfide-bonded Cys residues ($C_\alpha H$ C59-$C_{\beta\beta'}H$ C67, $C_{\beta\beta'}H$ C59-$C_\alpha H$ C67, $C_{\beta\beta'}H$ C59-$C_{\beta\beta'}H$ C67) observed in both solvent conditions, $C_\alpha H$ K62-$C_\beta H_3$ A66 in water (unobservable in TFE because of signal overlap) and $C_\alpha H$ K61-HN K64 in 30% TFE (unobservable in water because of signal overlap). Incorporation to the model structure calculations of dihedral ϕ and ψ angle constraints derived from the $^1H_\alpha$, $^{13}C_\alpha$ and $^{13}C_\beta$ chemical shifts (19 for ϕ and 10 for ψ in water and 20 for ϕ and 18 for ψ in 30% TFE) led to better model structure definition, but it did not modify their structural features (pair-wise RMSD for 50–68 backbone atoms goes from 2.1 ± 0.8 Å to 1.3 ± 0.4 Å in water, and from 1.0 ± 0.5 Å to 0.3 ± 0.1 Å in 30% TFE).

A better definition of the model structures in 30% TFE than in water was expected from the higher number of experimental constraints available in 30% TFE. However, the resulting structures in both solvents were very similar, as indicated by the fact that the pair-wise RMSD values of the structure ensemble including the best 20 TFE model structures and the best 20 water structures were approximately equivalent to the RMSD values obtained in aqueous solution. This indicates that the main features of the helical hairpin adopted by B-49-69 were the same in aqueous solution as in 30% TFE.

The model structures calculated for B-49-69 in either water or in 30% TFE (Figure 4) exhibit an α-helix spanning residues 50–61, approximately the same helix α_4 found in the intact bacteriocin AS-48, and a 5-residue helix (residues 64–68), corresponding to the *N*-terminus of the 12-residue helix α_5 in the intact bacteriocin AS-48. ϕ and ψ angles in B-49-69 and in the intact protein also show very close values, except for residues 49–50 at the *N*-terminus of helix α_4, residues 62–63 at the connecting loop, and residues 67–69 at the peptide *C*-terminus where helix α_5 ends in the designed B-49-69 and continues in the intact protein. The angle between the axis of the two helices in the B-49-69 helical hairpin is close to that in the intact protein (the average value for the 20 lowest energy B-49-69 model structures is $136° \pm 9°$ in water and $112° \pm 3°$ in 30% TFE, $117° \pm 2°$ in the intact protein in solution [6] and 115.4°, 117.5° and 117.3° in the reported bacteriocin crystal structures [8]).

Antibacterial Assays

Biological activity assays with B-49-69 were carried out against *Listeria monocytogenes* CECT 4032, selected for being the most susceptible organism to AS-48. The results obtained show that this peptide lacks activity either in solid or liquid media even when high concentrations were employed. However, the results suggest that B-49-69 may compete with bacteriocin AS-48 in the cells adsorption under the conditions of this experiment. So, to test whether B-49-69 neutralizes the bacteriolytic activity of AS-48, 110 µg of this peptide dissolved in distilled water or in *ortho*-phosphoric acid at pH 5 was deposited onto BHA plates seeded with the indicator strain and left at 4 °C for 2.5 h before treatment with AS-48. In both conditions, the

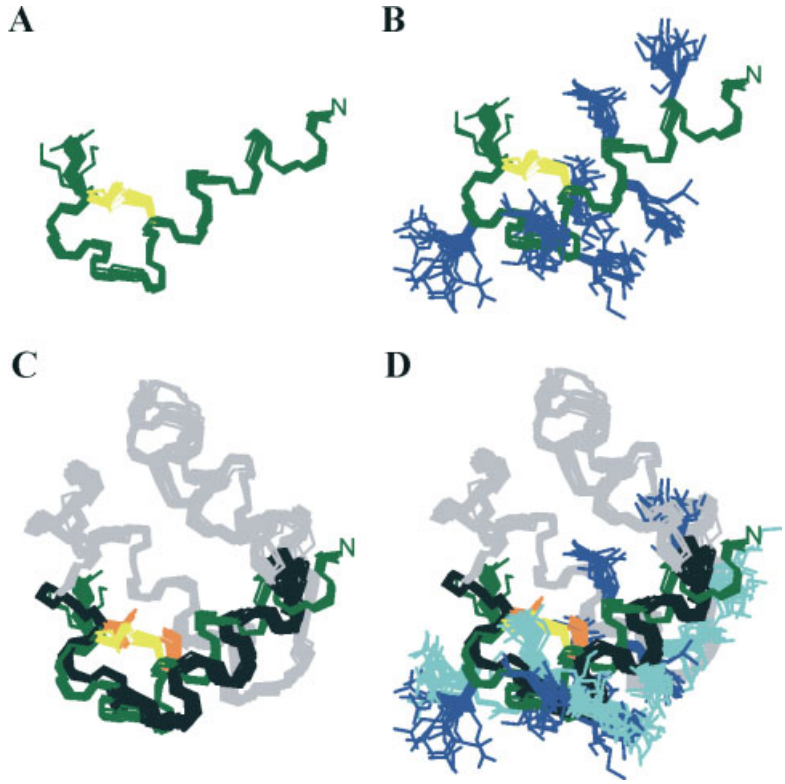

Figure 4 (Top) Superposition of the best 20 model structures calculated for B-49-69 in 30% TFE. (A) Backbone atoms are displayed in green and the disulfide bond in yellow. (B) Side chain atoms of Lys and Arg residues are displayed in blue. (Bottom) Structures of B-49-69 and intact bacteriocin AS-48 (pdb code: 1e68; [6]) superposed over the backbone atoms of residues 50–68. Backbone atoms are displayed in green for B-49-69, in black for segment 49–69 of bacteriocin AS-48 and in blue for all the other residues of bacteriocin AS-48. (C) Side chains of I59 and V67 residues in bacteriocin AS-48 are shown in orange and the C59-C67 disulfide bond of B-49-69 in yellow. (D) Side chains of Lys and Arg residues are displayed in blue for B-49-69 and in cyan for bacteriocin AS-48.

activity of bacteriocin AS-48 was partially neutralized, as demonstrated by the observed reduction of inhibition halos (Figure 5A). In the liquid medium, if B-49-69 was maintained in contact with the *L. monocytogenes* cells for 30 min, the effect of bacteriocin AS-48 was also partially neutralized during the next 2 h, as deduced from the decrease observed in the bacteriolytic effect (Figure 5B). When bacteriocin AS-48 was added prior to growing cells, its effect on the cell was very rapid, so further addition of B-49-69 had no consequence (data not shown). The observed effects were not comparable to those of inorganic cations [32] or organic salts [33,34]. For example, the activity of bacteriocin AS-48 was enhanced in the presence of sodium chloride [33].

Immunological Properties

To investigate whether B-49-69 shares some of the immunological properties of the native AS-48, a dot blot assay was carried out with specific antibodies anti-AS-48. The lack of colour in the spot corresponding to peptide B-49-69 to NC sheets indicated that the peptide was not recognized by the specific antibodies (in spite of the structural similitude of both peptides in this region) versus the positive reaction obtained with the AS-48 sample, used as a positive control (results not shown).

DISCUSSION

Bacteriocin AS-48 is highly active on different strains of *Listeria* which are far more sensitive to AS-48 than the rest of the Gram-positive bacteria reported previously [35]. The antibacterial activity of bacteriocin AS-48 has been proposed to occur by electrostatic interaction of its large positively charged patch localized at helices 4 and 5 with the negative charges at the surface of bacterial membranes [6]. The designed 21-residue fragment of bacteriocin AS-48, B-49-69, that comprises the highly positively charged region and displays the same secondary structure as the analogous region in the intact bacteriocin AS-48 does not conserve the inhibitory activity of the cyclic polypeptide, nor does it show the immunological properties of the native molecule. However, it appears to compete with bacteriocin AS-48 when added to exponential growth cultures of *L. monocytogenes* prior to bacteriocin but not when added after (see above). This suggests that, in

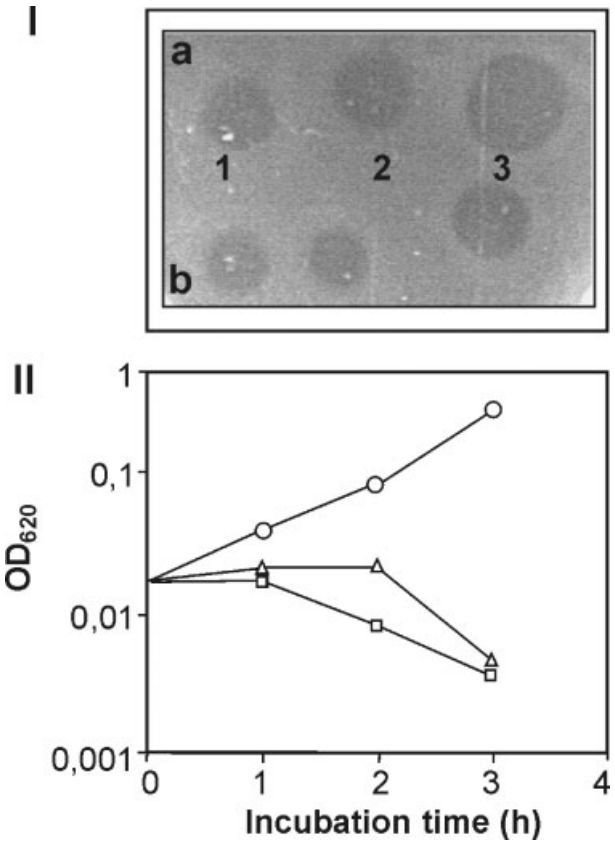

Figure 5 Neutralization of AS-48 activity against *Listeria monocytogenes* CECT 4032 by B-49-69. (A**)** In solid BHA media: drops containing B-49-69 (110 μg) at pH 5 (**1**) or pH 6.5 (**2**), plus 0.0625 μg (a) or 0.025 μg (b) of AS-48 were added to plates seeded with approx. 10^8 UFC *L. monocytogenes*. (**3**) Control of AS-48 activity without peptide B-49-69. (B**)** In liquid BHI media: exponentially grown *Listeria monocytogenes* cultures (approx. 10^7 UFC/ml) were added of 0.05 μg/ml of AS-48 (□) or 220 μg/ml of B-49-69 plus 0.05 μg/ml of AS-48 (Δ). (○) Culture control not treated.

the absence of bacteriocin AS-48, B-49-69 interacts with and binds to the negatively charged bacterial surface. The following describes a plausible mechanism compatible with these experimental observations. Once the bacterial surface is covered with the B-49-69 molecules, the approach of bacteriocin AS-48 (and likely, though not tested, of other antibacterial agents sharing the same mechanism of activity) is hindered, so that they can not proceed with the biological action of membrane permeation. When bacteriocin AS-48 is added first to a medium with bacteria cells, it binds very fast to the bacterial surface leading to the cell lysis, so that the subsequent addition of B-49-69 is ineffective. The designed B-49-69 appears to mimic the first stage of the activity of bacteriocin AS-48, that of binding to the cell surface, but once there it remains inoperative and is unable to carry out the final stage of the process, i.e. pore formation in the bacterial membrane. This is different to the behaviour of similar peptide domains of NK-lysin and granulysin, which were shown to be active against Gram-positive and Gram negative bacteria, and even with the NK-lysin peptide being active against *P. aeruginosa* and *S. aureus*, two organisms against which the parent molecule is inactive. These results suggest that the mechanism of membrane disruption by bacteriocin and the like is not always as simple as in the case of NK-lysin, in which a deposition of positively charged molecules on the plane of the bacterial membrane together with a sufficiently high potential across the bilayer leads to molecular electroporation [36]. As has been suggested, pore formation may require a certain distribution of the electrostatic and/or hydrophobic surfaces. In one of the models [6], once the polypeptide is bound to the membrane, hydrophobic patches on its belt would favour an accumulation of molecules of bacteriocin on the surface that would in turn favour electroporation. In the alternative model [8], hydrophobic patches surrounding the dimer DF-2 are needed for partial insertion into the membrane. Such a distribution of hydrophobic and hydrophilic surfaces is present in bacteriocin AS-48, but is absent in the simplified peptide B-49-69. In any case, the data suggest that the first step in the mechanism of antibacterial activity of bacteriocin AS-48 occurs by electrostatic interaction between the positively charged patch displayed by the protein and the negatively charged bacterial surface. Future work addressed to accomplish the goal of obtaining a minimal peptide with bacteriocin AS-48 antibiotic properties will greatly benefit from the results on B-49-69 which constitutes our first attempt towards it.

Supplementary Material

Two tables listing the ^{1}H and ^{13}C δ-values of B-49-69 (SM1 & SM2), available from the authors upon request.

Acknowledgements

We thank Mrs C. López and Mr L. de la Vega for technical assistance and Dr C. Alfonso for the sedimentation equilibrium experiments.

REFERENCES

1. Andreu D, Rivas L. Synthesis of antibiotic peptides. In *Peptide Antibiotics: Discovery, Modes of Action and Application*, Dutton CJ, Haxell MA, McArthur HAI, Wax RG (eds). Marcel Dekker: New York, 2001; 15–46.
2. Andreu D, Rivas L. Cecropin-melittin hybrid peptides as versatile templates in the development of membrane-active antibiotic agents. In *Pore-forming Peptides and Protein Toxins* Lazarovici P, Menestrina G, Dalla Serra M (eds). Harwood Academic: Reading, 2002; 215–259.
3. Samyn B, Martinez-Bueno M, Devreese B, Maqueda M, Galvez A, Valdivia E, Coyette J, Van Beeumen J. The cyclic structure of

the enterococcal peptide antibiotic AS-48. *FEBS Lett.* 1994; **352**: 87–90.
4. Martínez-Bueno M, Maqueda M, Gálvez A, Samyn B, Van Beeumen J, Coyette J, Valdivia E. Determination of the gene sequence and the molecular structure of the enterococcal peptide antibiotic AS-48. *J. Bacteriol.* 1994; **176**: 6334–6339.
5. Gálvez A, Máqueda M, Martinez-Bueno M, Valdivia E. Bactericidal and bacteriolytic action of peptide antibiotic AS-48 against gram-positive and gram-negative bacteria and other organisms. *Res. Microbiol.* 1989; **140**: 57–68.
6. González C, Langdon GM, Bruix M, Gálvez A, Valdivia E, Maqueda M, Rico M. Bacteriocin AS-48, a microbial cyclic polypeptide structurally and functionally related to mammalian NK-lysin. *Proc. Natl Acad. Sci. USA* 2000; **97**: 11 221–11 226.
7. Andersson M, Curstedt T, Jornvall H, Johansson J. An amphipathic helical motif common to tumourolytic polypeptide NK-lysin and pulmonary surfactant polypeptide SP-B. *FEBS Lett.* 1995; **362**: 328–332.
8. Sánchez-Barrena MJ, Martínez-Ripoll M, Gálvez A, Valdivia E, Maqueda M, Cruz V, Albert A. Structure of bacteriocin AS-48: from soluble state to membrane bound state. *J. Mol. Biol.* 2003; **334**: 541–549.
9. Andreu D, Carreno C, Linde C, Boman HG, Andersson M. Identification of an anti-mycobacterial domain in NK-lysin and granulysin. *Biochem. J.* 1999; **344**: 845–849.
10. Laue TM, Shak BD, Ridgeway TM, Pelletier SL. Computer aided interpretation of analytical sedimentation data for proteins. In *Analytical Ultracentrifugation in Biochemistry and Polymer Science*, Harding SE, Rowe AJ, Horton JC (eds). Royal Society of Chemistry: Cambridge, 1992; 90–125.
11. Aue WP, Bertholdi E, Ernst RR. Two-dimensional spectroscopy. Application to NMR. *J. Chem. Phys.* 1976; **64**: 2229–2246.
12. Rance M. Improved techniques for homonuclear rotating-frame and isotropic mixing experiments. *J. Magn. Reson.* 1987; **74**: 557–564.
13. Jeener J, Meier BH, Bachmann P, Ernst RR. Investigation of exchange processes by two-dimensional NMR spectroscopy. *J. Chem. Phys.* 1979; **71**: 4546–4553.
14. Kumar A, Ernst RR, Wüthrich K. A two-dimensional nuclear Overhauser enhancement (2D NOE) experiment for the elucidation of complete proton-proton cross-relaxation networks in biological macromolecules. *Biochem. Biophys. Res. Commun.* 1980; **95**: 1–6.
15. Redfield AG, Kuntz SD. Quadrature Fourier detection: Simple multiplex for dual detection. *J. Magn. Reson.* 1975; **19**: 250–259.
16. Bodenhausen G, Ruben DJ. Natural abundance nitrogen-15 NMR by enhanced heteronuclear spectroscopy. *Chem. Phys. Lett.* 1980; **69**: 185–189.
17. Bax A, Subramanian J. Sensitivity-enhanced two-dimensional heteronuclear shift correlation NMR spectroscopy. *J. Magn. Reson.* 1986; **67**: 565–570.
18. Spera S, Bax A. Empirical correlation between protein backbone conformation and Cα and Cβ ^{13}C NMR chemical shifts. *J. Am. Chem. Soc.* 1991; **113**: 5490–5492.
19. Wüthrich K, Billeter M, Braun W. Polypeptide secondary structure determination by nuclear magnetic resonance observation of short proton-proton distances. *J. Mol. Biol.* 1984; **180**: 715–740.
20. Wüthrich K. *NMR of Proteins and Nucleic Acids*. John Wiley & Sons: New York, 1986.
21. Jiménez MA, Muñoz V, Rico M, Serrano L. Helix stop and start signals in peptides and proteins. The capping box does not necessarily prevent helix elongation. *J. Mol. Biol.* 1994; **242**: 487–496.
22. Jiménez MA, Bruix M, González C, Blanco FJ, Nieto JL, Herranz J, Rico M. CD and ^{1}H-NMR studies on the conformational properties of peptide fragments from the *C*-terminal domain of thermolysin. *Eur. J. Biochem.* 1993; **211**: 569–581.
23. Santiveri CM, Rico M, Jiménez MA. ^{13}Cα and ^{13}Cβ chemical shifts as a tool to delineate β-hairpin structures in peptides. *J. Biomol. NMR* 2001; **19**: 331–345.
24. Wishart DS, Sykes BD, Richards FM. Relationship between nuclear magnetic resonance chemical shift and protein secondary structure. *J. Mol. Biol.* 1991; **222**: 311–333.
25. Merutka G, Dyson HJ, Wright PE. 'Random coil' ^{1}H chemical shifts obtained as a function of temperature and trifluoroethanol concentration for the peptide series GGXGG. *J. Biomol. NMR* 1995; **5**: 14–24.
26. Bartels C, Xia T, Billeter M, Güntert P, Wuthrich K. The program XEASY for computer-supported NMR spectral analysis of biological macromolecules. *J. Biomol. NMR* 1995; **6**: 1–10.
27. Guntert P, Mumenthaler C, Wuthrich K. Torsion angle dynamics for NMR structure calculation with the new program DYANA. *J. Mol. Biol.* 1997; **273**: 283–298.
28. Cornilescu G, Delaglio F, Bax A. Protein backbone angle restraints from searching a database for chemical shift and sequence homology. *J. Biomol. NMR* 1999; **13**: 289–302.
29. Koradi R, Billeter M, Wuthrich K. MOLMOL: a program for display and analysis of macromolecular structures. *J. Mol. Graph.* 1996; **14**: 51–55, 29–32.
30. Hawkes R, Niday E, Gordon J. A dot-immunobinding assay for monoclonal and other antibodies. *Anal. Biochem.* 1982; **119**: 142–147.
31. Maqueda M, Gálvez A, Martinez-Bueno M, Guerra I, Valdivia E. Neutralizing antibodies against the peptide antibiotic AS-48: immunocytological studies. *Antimicrob. Agents Chemother.* 1993; **37**: 148–151.
32. Gálvez A, Valdivia E, Martinez-Bueno M, Máqueda M. Induction of autolysis in *Enterococcus faecalis* S-47 by peptide A-47. *J. Appl. Bacteriol.* 1990; **69**: 406–413.
33. Abriouel H, Máqueda M, Gálvez A, Martínez-Bueno M, Valdivia E. Inhibition of bacterial growth, enterotoxin production, and spore outgrowth in strains of *Bacillus cereus* by bacteriocin AS-48. *Appl. Environ. Microbiol.* 2002; **68**: 1473–1477.
34. Ananou S, Valdivia E, Martínez Bueno M, Gálvez A, Máqueda M. Effect of combined physico-chemical preservatives on enterocin AS-48 activity against the enterotoxigenic *Staphylococcus aureus* CECT 976 strain. *J. Appl. Microbiol.* 2004; **97**: 48–56.
35. Mendoza F, Maqueda M, Gálvez A, Martínez-Bueno M, Valdivia E. Antilisterial activity of peptide AS-48 and study of changes induced in the cell envelope properties of an AS-48-adapted strain of *Listeria monocytogenes*. *Appl. Environ. Microbiol.* 1999; **65**: 618–625.
36. Miteva M, Andersson M, Karshikoff A, Otting G. Molecular electroporation: a unifying concept for the description of membrane pore formation by antibacterial peptides, exemplified with NK-lysin. *FEBS Lett.* 1999; **462**: 155–158.
37. Bundi A, Wüthrich K. ^{1}H-NMR parameters of the common amino acid residues measured in aqueous solution of linear tetrapeptides H-Gly-Gly-X-Ala-OH. *Biopolymers* 1979; **18**: 285–297.
38. Wishart DS, Bigam CG, Holm A, Hodges RS, Sykes BD. ^{1}H, ^{13}C and ^{15}N random coil NMR chemical shifts of the common amino acids. I. Investigations of nearest-neighbor effects. *J. Biomol. NMR.* 1995; **5**: 67–81.

